

Large cooperativity and microkelvin cooling with a three-dimensional optomechanical cavity

Mingyun Yuan, Vibhor Singh, Yaroslav M. Blanter, and Gary A. Steele*

Kavli Institute of NanoScience, Delft University of Technology,

PO Box 5046, 2600 GA, Delft, The Netherlands.

(Dated: October 19, 2015)

arXiv:1507.08898v2 [cond-mat.mes-hall] 16 Oct 2015

* g.a.steele@tudelft.nl

In cavity optomechanics, light is used to control mechanical motion. A central goal of the field is achieving single-photon strong coupling, which would enable the creation of quantum superposition states of motion. Reaching this limit requires significant improvements in optomechanical coupling and cavity coherence. Here, we introduce a new optomechanical architecture consisting of a silicon-nitride membrane coupled to a three-dimensional superconducting microwave cavity. Exploiting their large quality-factors, we achieve an optomechanical cooperativity of 146,000 and perform sideband cooling of the kilohertz-frequency membrane motion to 34 ± 5 microkelvin, the lowest mechanical mode temperature reported to date. The achieved cooling is limited only by classical noise of the signal generator, and should extend deep into the ground state with superconducting filters. Our results suggest that this new realisation of optomechanics has the potential to reach the regimes of ultra-large cooperativity and single-photon strong coupling, opening up a new generation of experiments.

In recent years, cavity optomechanics has been used to realise a wide range of exciting experiments with mechanical resonators, including achieving exquisite measurement precision [1–3], strong-coupling between the mechanical and cavity modes [4–6], cooling to the quantum ground state [7, 8], for microwave amplification [9, 10], to entangle propagating microwave photons with mechanical motion [11], for microwave photon storage [12, 13], to observe quantum backaction noise [14], to generate squeezed light [15, 16], and to transduce photons between the optical and microwave domains [17–19]. These successful experiments, performed in the regime of linear optomechanics, were enabled by improvements of the coherence of the optomechanical coupling between light and motion.

In linear optomechanics, the relevant figure of merit for the optomechanical coupling is a parameter called cooperativity. Cooperativity combines the optomechanical coupling rate g , the cavity decay rate κ , and the mechanical decay rate γ_m , into a dimensionless constant $C = \frac{4g^2}{\kappa\gamma_m}$ that quantifies the optomechanical system’s efficiency in exchanging photons and phonons [20]. It is similar to the Purcell factor in atomic physics (also often referred to as cooperativity) describing the coupling between cavity fields and atoms. An advantage of linear optomechanics is that compared to the single-photon coupling rate g_0 , the multiphoton coupling rate g is significantly enhanced, given by $g = \sqrt{N_d}g_0$ where N_d is the number of photons used to drive the cavity. The relevant limit for cooperativity in

quantum experiments is the so-called quantum coherent limit, in which the cooperativity is larger than the number of equilibrium thermal quanta in the mechanical resonator. In the quantum coherent limit, an exchange of a photon and phonon occurs faster than the time it takes for a phonon to leak into the mechanical resonator ground state from the thermal bath. Achieving higher cooperativity that is deeper in the quantum coherent limit in linear optomechanics would imply the ability to cool closer to the quantum ground state and the preparation of mechanical quantum states with high fidelity.

Beyond linear optomechanics, the field is striving to reach the limit of single-photon strong coupling, in which interaction of light and mechanical motion is coherent at the level of a single photon. In this limit, the single-photon coupling rate g_0 exceeds both the cavity decay rate κ and the mechanical decay rate γ_m ($g_0 > \kappa, \gamma_m$). If one could reach this limit, one could take advantage of the intrinsic non-linearity of the optomechanical coupling at the single-photon level to construct quantum superpositions of mechanical motion using optomechanics with classical light. In current experiments, $g_0 \ll \kappa$, and existing optomechanical implementations would require significant improvements in g_0 and/or κ to approach single-photon strong coupling.

Here, we present a new optomechanical architecture with large optomechanical coupling that can potentially reach the single-photon strong coupling limit. The design combines two highly coherent elements that are applied for the first time in the microwave optomechanics domain. The first element is a millimetre-sized, nanometre-thick high-stress silicon nitride (SiN_x) membrane, a technology that has demonstrated quality factors up to 1×10^7 at cryogenic temperatures [21]. Such membranes have been used extensively in the optical domain [14, 16, 22–24] and in transducer applications [18, 19], but have not yet been explored as an element in a pure microwave optomechanical system. The second optomechanical element is a three-dimensional (3D) microwave cavity, recently popular in the superconducting qubit community for their exceptional coherence times [25–27]. By combining these two highly coherent elements, we create a new optomechanical platform with large cooperativity, demonstrate cooling to the lowest mechanical mode temperature reported to date, and show that this new system has the potential to scale to couplings significantly beyond the state-of-the-art.

Results

Description and characterisation of the device. Fig. 1 illustrates the principle of this new 3D optomechanical platform. The mechanical resonator is made from high-stress SiN_x membrane (Fig. 1a) that is metallised with an Al electrode. The cavity itself is an aluminium box, Fig. 1b, in which electromagnetic fields are confined by superconducting walls in all three dimensions. Coupling to the motion of the membrane is achieved by using a flip-chip technique to place the membrane on top of antenna electrodes on a separate substrate, Fig. 1c-e. Fig. 1f shows an effective lumped-element circuit model of the assembled cavity and membrane. Optomechanical coupling results from the modulation of the effective shunt capacitance when the membrane displaces, changing the cavity frequency. From finite-element simulations, we estimate a single photon coupling rate of $g_0 = (d\omega_0/dx) \cdot x_{\text{zpf}} = 2\pi \times 0.36$ Hz, where ω_0 is the cavity mode frequency, x is the mechanical displacement of the membrane and x_{zpf} is the amplitude of its zero-point fluctuation. The simplicity of the assembly of this 3D cavity architecture also makes it attractive for implementing devices such as microwave-to-optical transducers [17–19] by potentially incorporating an optical fiber into the superconducting box.

Measurements are performed in a dilution refrigerator with a base temperature of $T_b = 13$ mK (see Supplementary Figure 1 and Supplementary Note 1). Fig. 2a shows a measurement of the reflection coefficient $|S_{11}|$ of the cavity. From a fit to the data, we find a total linewidth of $\kappa = 2\pi \times 45.5$ kHz, corresponding to a loaded quality factor of $Q_L = 1.1 \times 10^5$. From power dependence, we find a maximum intracavity photon occupation $N_{\text{max}} = 1.3 \times 10^8$ before the onset of a nonlinear response. The ratio $\eta = \kappa_e/\kappa \approx 0.48$ of the external decay rate κ_e and κ indicates that the cavity is slightly undercoupled (see Supplementary Figure 2 and Supplementary Note 2).

In Fig. 2b, we characterise the mechanical response of the membrane with the cavity using a resonant microwave tone injected at ω_0 . The thermomechanical motion of the membrane generates a peak in the sideband power spectral density (PSD) $S(\omega)$ of the microwave field leaving the cavity at a frequency offset $\Delta\omega = \omega_m$ from the carrier signal, shown in Fig. 2b. We find a mechanical resonance frequency of $\omega_m = 2\pi \times 123$ kHz, consistent with expected fundamental mode frequency of the membrane. A Lorentzian fit yields a linewidth of $\gamma_m = 2\pi \times 3.5$ mHz, corresponding to an ultra-high mechanical quality factor of $Q_m = 3.5 \times 10^7$, significantly higher than the typical $Q_m \lesssim 10^6$ of membranes used in optomechanical and transducer experiments.

Large cooperativity. To quantify the strength of the optomechanical coupling, in Fig. 3 we measure the cooperativity C between the mechanical resonator and the cavity. Together with initial phonon occupancy of the mechanical resonator n_m^i , several criteria can be conveniently expressed with C , such that for reaching the quantum ground state of motion, $C + 1 > n_m^i$, or for reaching the radiation pressure shot noise limit, $C > n_m^i(1 + (\frac{\omega_m}{\kappa})^2)$. To measure C , we use optomechanically-induced transparency (OMIT) [10, 28, 29], which allows one to directly determine the cooperativity with no free fit parameters. In OMIT, illustrated in Fig. 3a, the cavity is driven by a strong drive tone (ω_d) while a second weak probe (ω_p) is used to measure the cavity response. When driven on the red sideband ($\omega_d = \omega_0 - \omega_m$), a transparency window appears within the broad resonance dip of the cavity reflection coefficient [10]. In the limit $g \ll \kappa$, the linewidth of the transparency window in $|S_{11}|^2$ is given by $\gamma_m(C+1)$ and the peak value by $C/(C+1)$. Fig. 3b shows an example of an OMIT measurement with drive-photon number $N_d = 1.0 \times 10^8$: from the broadened linewidth of the feature together with its near unity transmission, we extract $C = 94,500$. Fig. 3c shows the extracted C for different drive powers: at the maximum power sustained by the cavity, we achieve $C_{\max} = 1.46 \times 10^5$.

Microkelvin cooling of the membrane resonator. The large cooperativity of our optomechanical setup is, in principle, capable of cooling deep into the quantum ground state of motion if the mode is thermalised to the temperature of the fridge ($\frac{k_B T_b}{C_{\max} \hbar \omega_m} = 0.015$). In order to demonstrate the cooling of the resonator, in Fig. 4 we use the spectral density of the thermomechanical sideband to directly observe the phonon occupation of the membrane. While driving the cavity on the red sideband, the output microwave PSD $S(\omega_0)$ at the cavity resonance frequency ω_0 is given by:

$$\frac{S(\omega_0)}{\hbar \omega_0} = \frac{S_{vv}(\omega_0)}{\mathcal{G} \hbar \omega_0} = 4\eta \frac{C}{(C+1)^2} \left(n_m^i + \frac{1}{2} \right) + n_{\text{add}} \quad (1)$$

where $S_{vv}(\omega_0)$ is the measured microwave PSD on the spectrum analyser, \mathcal{G} is the net gain of the signal path from the output of the cavity to the input of the spectrum analyser, and n_{add} is the added photon noise quanta from the amplification chain referenced to the output of the cavity. By varying the bath temperature T_b and measuring $S_{vv}(\omega)$, we obtain an absolute calibration of \mathcal{G} , n_{add} , and n_m^i (details provided in Supplementary Figure 3 and Supplementary Note 3, 4). At the base temperature of the refrigerator, we find that the membrane is thermalised to $T_m^i \approx 180$ mK, corresponding to $n_m^i \approx 3.06 \times 10^4$. From the

thermal calibration, we also extract $g_0 = 2\pi \times 0.22$ Hz, in good agreement with simulations (Supplementary Figure 4 and Supplementary Note 5).

Fig. 4a shows $S(\omega)$ for different cooperativities C of the cooling tone. As C increases, $S(\omega_0)$ from the thermomechanical noise peak decreases, indicating that the mode temperature of the mechanical resonator is reduced. At larger cooling powers, however, although $S(\omega_0)$ continues to drop, the noise floor of $S(\omega)$ outside the mechanical bandwidth begins to increase, and the peak in the PSD becomes a dip (bottom two panels of Fig. 4a). The increase in the noise floor is an indication of noise fluctuations of the cavity field [7]. Due to correlations between the fluctuations of the cavity and of the mechanical resonator, the spectrum shows a suppression of the total PSD at the cavity frequency [30].

In order to extract the mechanical occupation factor in the presence of cavity noise, it is no longer sufficient to look only at $S(\omega_0)$. In particular, with sufficiently large C (and in the absence of other sources of heating that would increase n_m^i such as losses in the superconducting film or in the dielectric membrane or substrate), $S(\omega_0)$ drops to the amplifier noise floor independent of the amount of cavity noise (Eq. 1). This does not, however, imply that the mechanical mode is at zero temperature: due to the hybridisation of the mechanical and optical fields, the final mechanical mode occupation in the presence of cavity noise is given by (Supplementary Note 6):

$$n_m = \frac{1}{(C+1)}n_m^i + \frac{C}{(C+1)}n_c \quad (2)$$

where n_c is the cavity noise power measured in energy quanta. In order to find the final occupation n_m , one must also determine n_c . In the limit $g \ll \kappa$, cavity noise appears as an increase in the noise floor outside of the mechanical sideband (green dashed line in Fig. 4a) with a spectral density (see Supplementary Note 6 for the more general equation of $S(\omega)$):

$$\frac{S(\omega_0 + \delta\omega)}{\hbar\omega} = 4\eta \left(n_c + \frac{1}{2} \right) + n_{\text{add}} \quad (3)$$

where $(C+1)\gamma_m \ll \delta\omega \ll \kappa$. From this expression, one can extract the cavity occupation n_c and consequently n_m for all powers, shown in Fig. 4b. As C is increased, we find that n_m drops initially to a value of 5.2 ± 0.7 , corresponding to a mode temperature of 34 ± 5 μK , beyond which the mechanical occupation begins to increase sharply due to heating from cavity noise. The temperature reported here is roughly a factor of two lower than recent experiments in the optical domain with silicon nitride membranes [23, 24] due to the very low frequency of our membrane.

Although the large cooperativity in our experiment should allow us to cool the membrane to $n_m = 0.2$ given the initial thermal occupation, in practice we are limited to $n_m = 5.2 \pm 0.7$ by cavity noise. In order to cool to lower occupation in future experiments, it is important to identify the source of this cavity noise. The green line in Fig. 4b shows the expected n_c due to the carrier sideband noise of our microwave signal generator (Supplementary Note 7). The good agreement with the observed cavity noise data suggests that our final occupation is limited by the spectral purity of the microwave tone used for the sideband cooling.

Discussion

Having demonstrated the lowest temperature $T_m = 34 \mu\text{K}$ reported to date for a mechanical resonator, we analyse the potential of this new implementation to reach the deep quantum coherent coupling limit. In the current experiment, the cooling is limited by the classical sideband noise of the signal generator. Removing this noise with a tunable superconducting cavity with a linewidth of 10 kHz would already provide sufficient suppression to cool to a final occupation of 0.2. A second approach would be to increase g_0 by shrinking the capacitor gap: reducing the membrane-antenna gap from 3 μm to 100 nm would increase g_0 by a factor of 10^3 and C_{max} by 10^6 . A third approach is to improve the cavity linewidth [27], also yielding higher cooperativity at lower photon numbers. Finally, combining a smaller gap ($g_0 \sim 300 \text{ Hz}$) with a better cavity ($\kappa \sim 10 \text{ Hz}$) could yield ultra-high cooperativities $C > 10^{12}$. Such a fully optimised design would also achieve single-photon strong coupling ($g_0 > \kappa, \gamma_m$) [31, 32], enabling preparation and detection of non-classical states of motion such as Fock states or Schrödinger cat states with optomechanics.

In conclusion, we have developed a novel optomechanical system coupling the motion of a millimetre-sized membrane to a 3D microwave cavity. Exploiting the high coherence of the membrane and of the cavity, we achieve a cooperativity of $C > 1.4 \times 10^5$ and perform sideband cooling of the millimetre-size membrane to 34 μK , corresponding to a thermal occupation $n_m = 5.2$. The scaling of this 3D optomechanical system offers the possibility to reach optomechanical couplings far beyond the state-of-the-art, potentially entering the single-photon strong coupling regime in which a new generation of quantum experiments with mechanical objects would become possible.

Acknowledgments We would like to thank S. J. Bosman, S. Yanai, S. Gröblacher, L. DiCarlo, D. Ristè and R. Hoogerheide for discussions and support. Fabrication is carried out in Kavli Nanolab and this project is supported by the Stichting voor Fundamenteel Onderzoek der Materie (FOM).

Author Contribution G. A. S. conceived the device and supervised the project. M. Y. prepared the devices. M. Y. and V. S. set up the experiment and performed the measurements. M. Y., V. S. and G. A. S. analysed the data. M. Y. and Y. M. B. performed the theoretical calculation. All authors contributed to writing of the manuscript.

Methods

Device preparation. We use commercial SiN_x membranes manufactured by Norcada. The membranes have the dimensions of $50 \text{ nm} \times 1 \text{ mm} \times 1 \text{ mm}$, and are supplied with a $5 \text{ mm} \times 5 \text{ mm}$ Si frame. We deposit a 20 nm thick film of Al on top of the membrane without covering the clamping edges by using a physical mask. On a separate sapphire substrate, we pattern two Al antenna pads with 80 nm of Al followed by the deposition of SiN_x spacer layer. To ensure the membrane does not come into contact with the substrate, a recess of 100 nm is etched. The metallised SiN_x membrane is then placed on top of the antenna pads to form a capacitor using a vacuum pick-and-place technique. A single drop of $0.1 \mu\text{l}$ of 2-part epoxy is applied on the substrate to attach one corner of the membrane's Si frame to the substrate. Using the depth of focus to locate the vertical position of the membrane and of the bottom antenna pads while looking through the membrane with an optical microscope, we estimate the gap to be approximately $3 \mu\text{m}$. The gap is much larger than that designed in the spacer, most likely due to contamination from dust in the large contact area between the Si frame of the membrane and the substrate. The 3D microwave cavity is formed by closing two halves of a machined block made out of 6061-aluminium. The inner surface of the cavity is polished using a polishing paste, but is not chemically etched. The cavity is assembled by screwing the two halves of the cavity together with no sealing mechanism. The dimension of the whole cavity is $28 \text{ mm}(\mathbf{x}) \times 28 \text{ mm}(\mathbf{y}) \times 8 \text{ mm}(\mathbf{z})$, with rounded corners of radius 1 mm in the \mathbf{y} - \mathbf{z} plane.

Measurement. The bare frequency of the cavity without the antenna substrate and mem-

brane is 7.4 GHz. The membrane attached to the antenna is placed at the centre of the cavity, coupling to the TE_{110} mode. We estimate the total mass of the membrane including the Al layer to be $m = 200$ ng, corresponding to an estimated quantum zero-point fluctuation of $x_{zpf} = 0.6$ fm. Measurements are performed in a cryogen free dilution refrigerator. To minimise cavity instability during the measurements, the sample is mounted on a mass-spring vibration isolation stage on the mixing chamber with resonance frequency of ~ 1 Hz. During the cooling measurements, the pulse tube is temporarily turned off to minimise vibrations of the sample and the cables. Measurements are started 1.5 minutes after the switch-off and performed in a ~ 2 minute window before the temperature of the mixing chamber begins to increase.

-
- [1] Teufel, J. D., Donner, T., Castellanos-Beltran, M. A., Harlow, J. W. & Lehnert, K. W. Nanomechanical motion measured with an imprecision below that at the standard quantum limit. *Nature Nanotechnology* **4**, 820–823 (2009).
 - [2] Anetsberger, G. *et al.* Measuring nanomechanical motion with an imprecision below the standard quantum limit. *Physical Review A* **82**, 061804 (2010).
 - [3] Wilson, D. J. *et al.* Measurement and control of a mechanical oscillator at its thermal decoherence rate. Preprint at: <http://arXiv.org/abs/1410.6191> (2014).
 - [4] Gröblacher, S., Hammerer, K., Vanner, M. R. & Aspelmeyer, M. Observation of strong coupling between a micromechanical resonator and an optical cavity field. *Nature* **460**, 724–727 (2009).
 - [5] Teufel, J. D. *et al.* Circuit cavity electromechanics in the strong-coupling regime. *Nature* **471**, 204–208 (2011).
 - [6] Verhagen, E., Deléglise, S., Weis, S., Schliesser, a. & Kippenberg, T. J. Quantum-coherent coupling of a mechanical oscillator to an optical cavity mode. *Nature* **482**, 63–67 (2012).
 - [7] Teufel, J. D. *et al.* Sideband cooling of micromechanical motion to the quantum ground state. *Nature* **475**, 359–363 (2011).
 - [8] Chan, J. *et al.* Laser cooling of a nanomechanical oscillator into its quantum ground state. *Nature* **478**, 89–92 (2011).
 - [9] Massel, F. *et al.* Microwave amplification with nanomechanical resonators. *Nature* **480**,

- 351–354 (2011).
- [10] Singh, V. *et al.* Optomechanical coupling between a multilayer graphene mechanical resonator and a superconducting microwave cavity. *Nat. Nanotechnol.* **9**, 820–824 (2014).
 - [11] Palomaki, T. A., Teufel, J. D., Simmonds, R. W. & Lehnert, K. W. Entangling mechanical motion with microwave fields. *Science* **342**, 710–713 (2013).
 - [12] Palomaki, T. A., Harlow, J. W., Teufel, J. D., Simmonds, R. W. & Lehnert, K. W. Coherent state transfer between itinerant microwave fields and a mechanical oscillator. *Nature* **495**, 210–214 (2013).
 - [13] Zhou, X. *et al.* Slowing, advancing and switching of microwave signals using circuit nanoelectromechanics. *Nature Physics* **9**, 179–184 (2013).
 - [14] Purdy, T. P., Peterson, R. W. & Regal, C. A. Observation of radiation pressure shot noise on a macroscopic object. *Science* **339**, 801–804 (2013).
 - [15] Safavi-Naeini, A. H. *et al.* Squeezed light from a silicon micromechanical resonator. *Nature* **500**, 185 – 189 (2013).
 - [16] Purdy, T. P., Yu, P.-L., Peterson, R. W., Kampel, N. S. & Regal, C. A. Strong optomechanical squeezing of light. *Phys. Rev. X* **3**, 031012 (2013).
 - [17] Bochmann, J., Vainsencher, A., Awschalom, D. D. & Cleland, A. N. Nanomechanical coupling between microwave and optical photons. *Nature Physics* **9**, 712–716 (2013).
 - [18] Andrews, R., Peterson, R. & Purdy, T. Bidirectional and efficient conversion between microwave and optical light. *Nature Phys.* **10**, 321–326 (2014).
 - [19] Bagci, T. *et al.* Optical detection of radio waves through a nanomechanical transducer. *Nature* **507**, 81–85 (2014).
 - [20] Aspelmeyer, M., Kippenberg, T. J. & Marquardt, F. Cavity optomechanics. *Rev. Mod. Phys.* **86**, 1391–1452 (2014).
 - [21] Zwickl, B. M. *et al.* High quality mechanical and optical properties of commercial silicon nitride membranes. *Appl. Phys. Lett* **92**, 103125 (2008).
 - [22] Thompson, J. D. *et al.* Strong dispersive coupling of a high-finesse cavity to a micromechanical membrane. *Nature* **452**, 72–75 (2008).
 - [23] Purdy, T. P. *et al.* Optomechanical raman-ratio thermometry. Preprint at: <http://arxiv.org/abs/1406.7247> (2014).
 - [24] Lee, D. *et al.* Observation of quantum motion in a nanogram-scale object. Preprint at:

- <http://arxiv.org/abs/1406.7254> (2014).
- [25] Paik, H. *et al.* Observation of high coherence in Josephson junction qubits measured in a three-dimensional circuit QED architecture. *Phys. Rev. Lett.* **107**, 240501 (2011).
 - [26] Kirchmair, G. *et al.* Observation of quantum state collapse and revival due to the single-photon kerr effect. *Nature* **495**, 205–209 (2013).
 - [27] Reagor, M. *et al.* Reaching 10ms single photon lifetimes for superconducting aluminum cavities. *Appl. Phys. Lett.* **102**, 192604 (2013).
 - [28] Weis, S. *et al.* Optomechanically induced transparency. *Science* **330**, 1520–1523 (2010).
 - [29] Agarwal, G. S. & Huang, S. Electromagnetically induced transparency in mechanical effects of light. *Phys. Rev. A* **81**, 041803 (2010).
 - [30] Poggio, M., Degen, C. L., Mamin, H. J. & Rugar, D. Feedback cooling of a cantilever’s fundamental mode below 5 mk. *Phys. Rev. Lett.* **99**, 017201 (2007).
 - [31] Rabl, P. Photon blockade effect in optomechanical systems. *Phys. Rev. Lett.* **107**, 063601 (2011).
 - [32] Nunnenkamp, A., Børkje, K. & Girvin, S. M. Single-photon optomechanics. *Phys. Rev. Lett.* **107**, 063602 (2011).

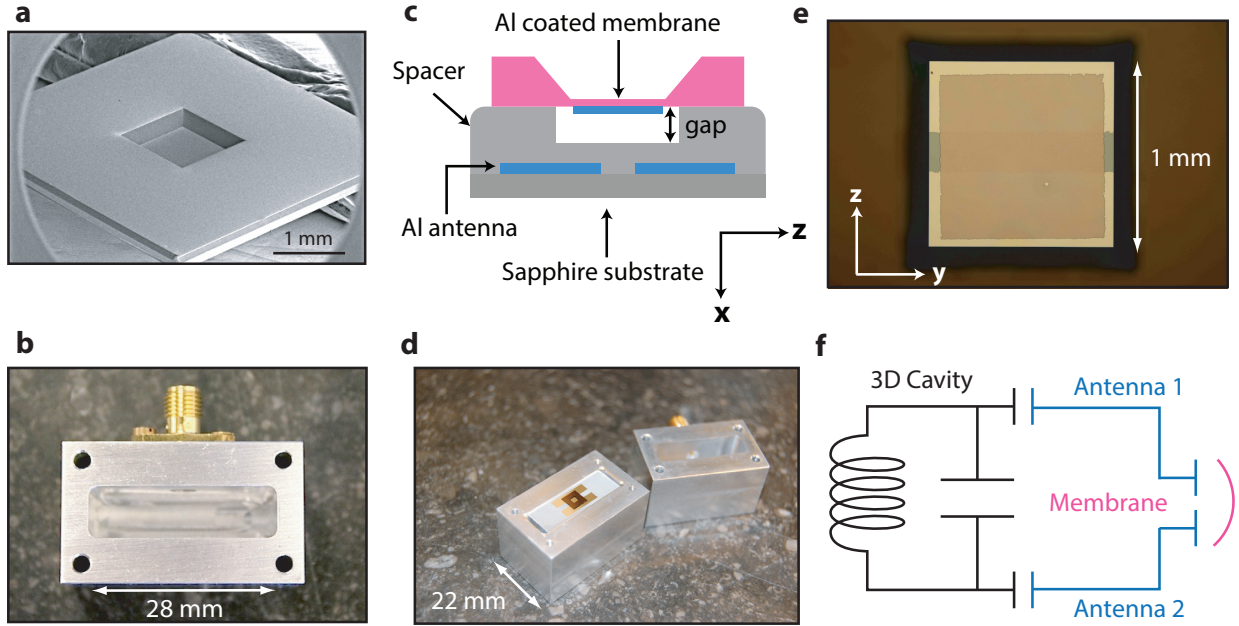


FIG. 1. **Microwave optomechanics with a 3D superconducting cavity and a millimetre-sized membrane.** **a**, Electron microscope image of a 50 nm thick SiN_x membrane. **b**, One half of the Al cavity with an SMA connector for reflection measurements. The dimensions of the cavity are $28 \times 28 \times 8$ in millimetre. **c**, Schematic showing the placement of the membrane over the antenna pads. The Al coating of the membrane forms a capacitor with the antennas below. **d**, A complete assembly. The membrane is positioned in the centre of the cavity, supported by a sapphire substrate patterned with the Al antenna. **e**, An optical microscope image looking from the top showing the Al-coated membrane and the underlying antenna pads. **f**, Effective lumped element model of the cavity and membrane. By changing the effective shunt capacitance, the frequency of the 3D cavity is modulated by the mechanical motion of the membrane.

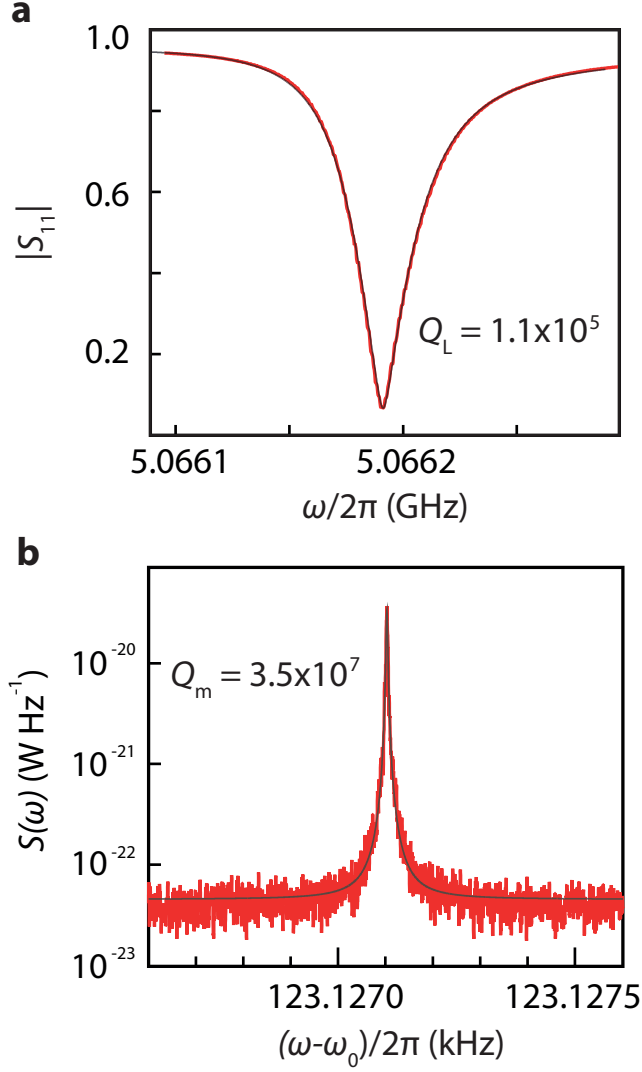


FIG. 2. **High quality-factors of the microwave cavity and mechanical resonator.** **a**, Reflection coefficient $|S_{11}|$ measurement of the cavity. The loaded quality factor is $Q_L = 1.1 \times 10^5$, corresponding to a total decay rate $\kappa = 2\pi \times 45.5$ kHz. Internal dissipation rate is $\kappa_0 = 2\pi \times 23.9$ kHz, with $Q_0 = 2 \times 10^5$. **b**, Power spectral density of the thermomechanical motion of the fundamental mode of the membrane $\omega_m \approx 2\pi \times 123$ kHz with linewidth $\gamma_m = 2\pi \times 3.5$ mHz, corresponding to $Q_m = 3.5 \times 10^7$. Red: data, Grey: fit.

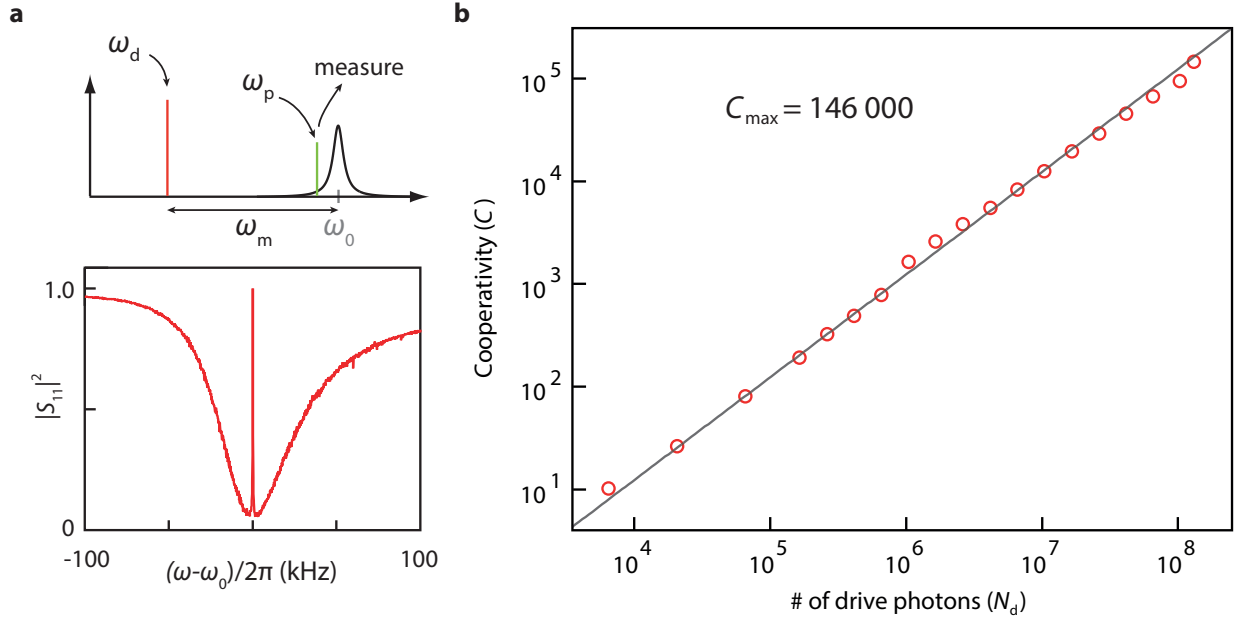


FIG. 3. **Large cooperativity measured with optomechanically-induced transparency (OMIT).** **a**, Illustration showing the OMIT measurement scheme. The cavity reflection coefficient S_{11} is measured with a weak probe tone (ω_p) while driving the cavity with a second strong tone near the red sideband ($\omega_d = \omega_0 - \omega_m$). A window of transparency appears in the cavity resonance (lower panel) with a width set by the mechanical linewidth. **b**, Extracted cooperativity C vs. driving photon number N_d . Grey line: expected linear scaling $C = \frac{4g_0^2 N_d}{\gamma_m \kappa}$. At maximum N_d , the cooperativity reaches $C_{\max} = 1.46 \times 10^5$, corresponding to $g_{\max} = 2\pi \times 2.5$ kHz.

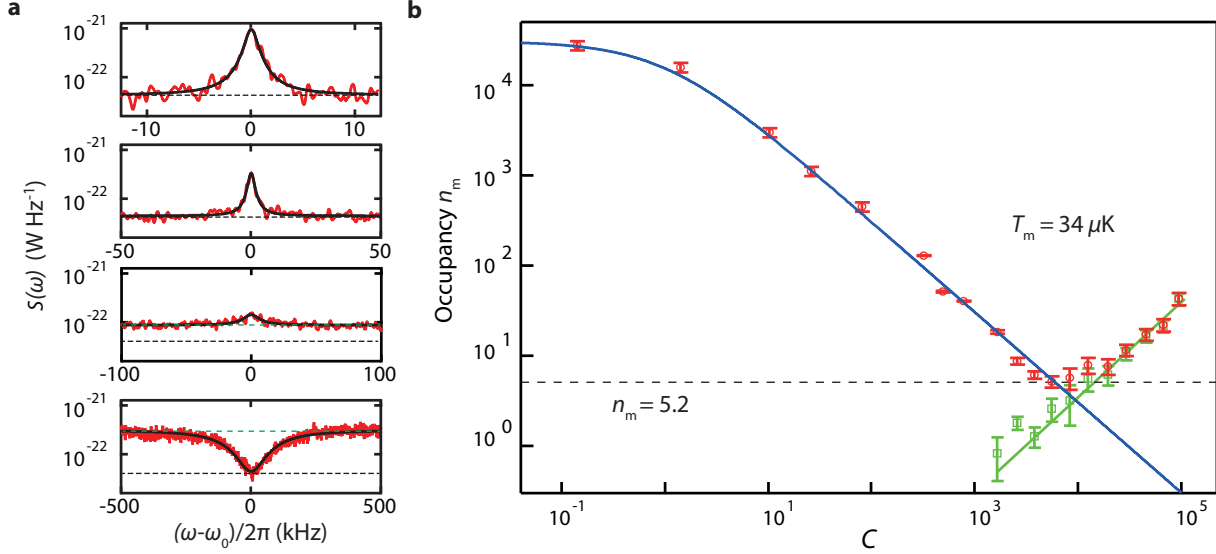
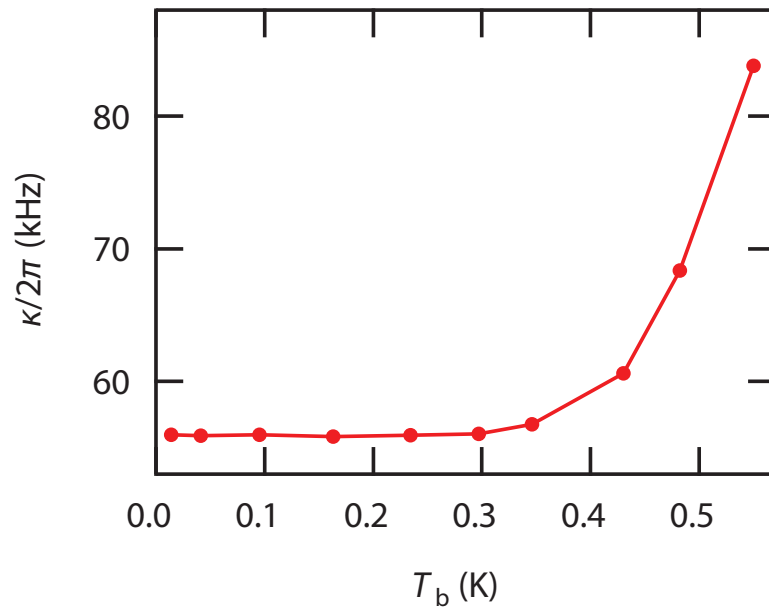
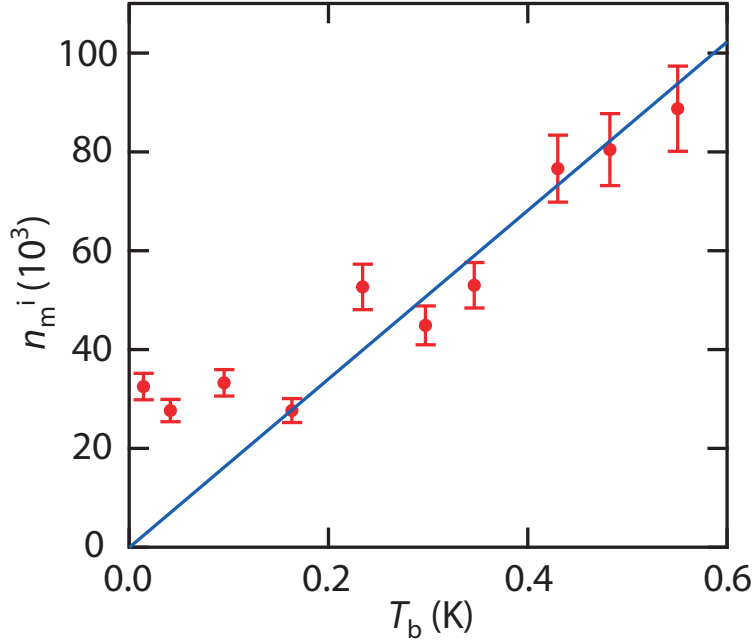


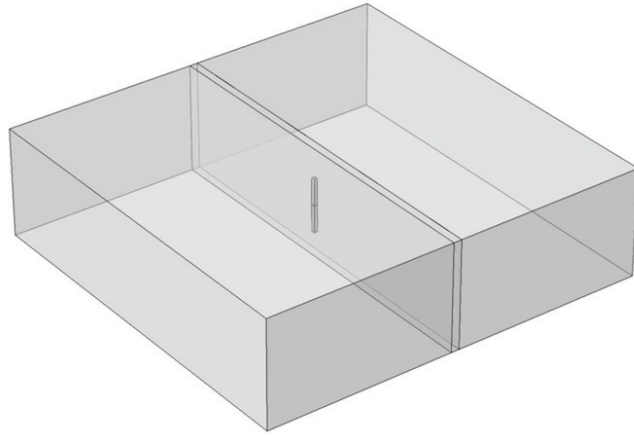
FIG. 4. **Microkelvin cooling of a millimetre-sized mechanical resonator.** **a**, Measured microwave PSD $S(\omega)$ with red-sideband driving (top to bottom: $C = 324, 785, 3810, 94500$). Black dashed line: noise floor n_{add} of the amplifier chain. As the cooperativity C of the cooling tone is increased, $S(\omega_0)$ is reduced and the mechanical linewidth is broadened. Initially, the thermal noise of the membrane appears as a peak with decreasing height. At higher C (lower two panels), the noise floor outside of the mechanical linewidth (green dashed line) begins to increase above n_{add} , indicating the presence of cavity noise. In the lowest panel, the output noise of the cavity is suppressed at ω_0 due to correlations of the mechanical and cavity fluctuations. From the thermal peak and the cavity noise background level (green dashed line), we extract both n_m and n_c for all cooling powers, shown in **b**. As a function of C , the mechanical occupancy n_m (red circle) drops, closely following $\frac{n_m^i}{C+1}$ (blue line) until the onset of cavity noise n_c (green squares) limits the final occupancy to a minimum of $n_m = 5.2$, corresponding to $T_m = 34 \mu\text{K}$. The error bars indicate the uncertainty of the data points and are calculated with the errors from the Lorentzian fit. The green line in **b** shows the expected n_c from the measured carrier sideband noise of the microwave generator.



Supplementary Figure 2. Cavity decay rate κ as a function of cryostat base temperature T_b . The line width of the cavity resonance starts to increase above 0.34 K.



Supplementary Figure 3. Calibration of the initial thermal occupancy n_m^i by varying the refrigerator temperature T_b . The mode temperature of the membrane is thermalised at base temperature to $T_m^i \approx 180$ mK, corresponding to $n_m^i \approx 3.06 \times 10^4$. The error bars indicate the uncertainty of the data points, combining the fluctuations due to the temperature and the signal level.



Supplementary Figure 4. COMSOL model showing a 3D cavity embedding an antenna.

Supplementary Note 1: Experimental setup

The sample is cooled down in a cryogen-free dilution refrigerator to a base temperature of 12 to 13 mK. Input microwave signals are attenuated at each thermal stage as illustrated by Supplementary Figure 1. At base temperature, the signal is injected into the cavity via the coupling port of a 20 dB directional coupler. The reflected power collected at the output port is amplified by a cold amplifier at the 3 K plate and subsequent amplifiers at room temperature and then detected by a network analyser or a spectrum analyser. Circulators are placed between the sample and the cold amplifier to isolate the sample from noise generated by the amplifier. A cancelling tone is applied using a directional coupler, a phase shifter and a continuous attenuator in order to reduce the amplitude of the strong drive tone before sending it to the room temperature amplifier. For the optomechanically-induced transparency (OMIT) experiment, a network analyser is used to generate the weak probe tone ω_p and a separate phase locked signal generator provides the strong drive tone ω_d .

Supplementary Note 2: Cavity characterisation

The cavity response $|S_{11}|$ in Fig. 2a in the main text is fitted with the following equation, taking into consideration the finite isolation of the directional coupler [1]:

$$|S_{11}(\omega)| = \left| \alpha e^{i\phi} + (1 - \alpha) \left(1 - \frac{\kappa_e}{i(\omega - \omega_0) + \frac{\kappa}{2}} \right) \right|, \quad (1)$$

where α is the isolation of the directional coupler.

Due to the low superconducting transition temperature of aluminium $T_c \sim 1.2$ K, the internal cavity quality factor is significantly reduced as the cryostat temperature T_b is raised above ~ 0.34 K, and the line width κ is broadened, as shown in Supplementary Figure 2. This effect needs to be taken into account in the thermal calibration. As a function of temperature, we find that κ_e remains constant.

Supplementary Note 3: Calibration of the mode temperature

A thermal calibration is carried out to determine the initial (i.e. without cooling) phonon occupancy $n_m^i = \frac{1}{\exp\left(\frac{\hbar\omega_m}{k_B T_m^i}\right) - 1}$ of the mechanical resonator, k_B being the Boltzmann constant and T_m^i the initial mode temperature. We send in a carrier signal at ω_0 to avoid any back-

action effects and measure the total power of its mechanical sideband at different cryostat temperature T_b . The total power generated by the thermal motion of the membrane is then used to extract the mechanical mode temperature T_m^i . We use a resolution bandwidth (RBW) of 1 Hz. In the limit of $\text{RBW} \gg \gamma_m$, the total thermal power can be directly read out from the peak height. For $T_b > 0.34$ K, ω_0 and κ changes significantly due to the low critical temperature of Al, which has to be taken into account. We plot the converted n_m^i as a function of refrigerator temperature T_b in Supplementary Figure 3. From the fitting line that passes the original point, at the base temperature the membrane is thermalised to $T_m^i \approx 180$ mK and $n_m^i \approx 3.06 \times 10^4$. The mode temperature is significantly higher than the base temperature of the refrigerator, which is probably an inevitable challenge one is faced with when working with a low-frequency (< 1 MHz) mechanical resonator.

Supplementary Note 4: Power calibration

The photon number in the cavity corresponding to the input power at the cavity P_{in} at frequency ω is calculated with

$$N = \frac{P_{\text{in}}}{\hbar\omega} \cdot \frac{\kappa_e}{\left(\frac{\kappa}{2}\right)^2 + (\omega - \omega_0)^2}. \quad (2)$$

While driving the cavity on resonance, the sideband power due to the thermal motion is expressed as

$$\begin{aligned} P_{\text{side}} &= P_{\text{in}} \left(\frac{g_0}{x_{\text{zpf}}} \right)^2 \cdot \frac{k_B T}{m\omega_m^2} \cdot \frac{\left(\frac{\kappa_e}{2}\right)^2}{\left(\frac{\kappa}{2}\right)^2 + (\omega - \omega_{r,b})^2} \frac{1}{\left(\frac{\kappa}{2}\right)^2 + (\omega - \omega_0)^2} \\ &= P_{\text{in}} \cdot g_0^2 \cdot 2n_m \cdot \frac{\left(\frac{\kappa_e}{2}\right)^2}{\left(\frac{\kappa}{2}\right)^2 + (\omega - \omega_{r,b})^2} \frac{1}{\left(\frac{\kappa}{2}\right)^2 + (\omega - \omega_0)^2}, \end{aligned} \quad (3)$$

where g_0 is again the single-photon coupling rate, k_B the Boltzmann constant and n_m the mechanical occupancy. The sideband frequency of interest is either ω_r or ω_b .

The loss of the input line \mathcal{L} and the gain of the output line \mathcal{G} are calibrated as the following: while driving the cavity on resonance ($\omega = \omega_0$) with power P'_{in} from the signal generator, the thermomechanical power measured by the spectrum analyser at the mechanical sidebands can be written as:

$$\begin{aligned} P_{\text{side}} &= P'_{\text{in}} \cdot g_0^2 \cdot 2n_m \left(\frac{\kappa_e}{\kappa} \right)^2 \frac{1}{\left(\frac{\kappa}{2}\right)^2 + \omega_m^2} \cdot \mathcal{L} \cdot \mathcal{G} \\ &= P'_{\text{in}} \cdot g_0^2 \cdot \beta. \end{aligned} \quad (4)$$

The combined value of $\mathcal{L} \cdot \mathcal{G}$ is determined by the network analyser. Thermal occupation can be measured by sweeping the bath temperature as described in the previous section. All the parameters being known in β , single-photon coupling strength g_0 can be extracted. This is equivalent to the single-photon coupling strength calibration the frequency modulation (FM) technique described in [8], where the FM peak of the carrier wave provides a side-by-side reference of $\mathcal{L} \cdot \mathcal{G}$. Using this approach, we measure the single-photon coupling strength to be $g_0 = 0.22$ Hz. This further allows us to calibrate the corresponding photon number N by using the experimentally obtained photon-enhanced $g = g_0\sqrt{N}$ (from cooperativity measurements). Subsequently, by rewriting Supplementary Equation 2 as

$$N = \frac{P'_{\text{in}}}{\hbar\omega} \cdot \frac{\kappa_e}{\left(\frac{\kappa}{2}\right)^2 + (\omega - \omega_0)^2} \cdot \mathcal{L}, \quad (5)$$

we calibrate the total input attenuation $\mathcal{L} = 70$ dB and correspondingly the output gain $\mathcal{G} = 73.5$ dB. The added noise of the output chain is calibrated to be $n_{\text{add}} = 12$ corresponding a noise temperature of approximately 2.6 K.

Supplementary Note 5: COMSOL RF simulations to estimate g_0

To estimate the single-photon coupling rate g_0 of the 3D-cavity-membrane system, we model the problem with a “variable capacitor in cavity” structure and numerically calculate the cavity frequency ω_0 with COMSOL. The following relation is used to derive g_0 :

$$g_0 = \frac{\delta\omega_0}{\delta C_1} \cdot \delta C_2 \quad (6)$$

where δC_1 is the change in capacitance by varying the gap between the two antenna rods, $\delta\omega_0$ the subsequent frequency shift and δC_2 the change in capacitance due to zero-point fluctuation x_{zpf} of the membrane. δC_2 can be expressed as $\delta C_2 = \frac{\epsilon_0 A_2}{d^2} x_{\text{zpf}}$, where ϵ_0 is the free space permittivity, A_2 the area of the membrane and d the gap between the membrane and the antenna.

The geometry of the COMSOL model is shown in Supplementary Figure 4. The dimension of the 3D cavity is 28 mm×28 mm×8 mm. There is a 0.6 mm thick sapphire substrate at the centre of the cavity. The antenna is simplified to two Al rods with a cross section of 0.25 mm×0.25 mm, the length of the antenna being 4 mm and their gap is varied between 20 and 30 μm , changing the parallel-plate capacitance between them. Although this geometry is different from the actual geometry of the antenna, it results in comparable

frequency pull of ω_0 , indicating that the capacitance participation ratio in the equivalent lumped-element circuit is similar. For a membrane of $1 \text{ mm} \times 1 \text{ mm}$, a gap of $d = 3 \text{ }\mu\text{m}$ and $x_{\text{zpf}} = 0.6 \text{ fm}$ the resulting coupling strength is $g_0 \approx 0.36 \text{ Hz}$. Since g_0 is inversely proportional to the square of d , if d can be reduced to 30 nm , g_0 can be increased to 3.6 kHz .

Supplementary Note 6: Quantum noise of optomechanical cooling

The linearised Hamiltonian of the optomechanical system in a frame rotating at the drive tone frequency ω_d can be written as [2–6]:

$$\hat{H} = -\hbar\Delta\hat{a}^\dagger\hat{a} + \hbar\omega_m\hat{b}^\dagger\hat{b} - \hbar g(\hat{a}^\dagger + \hat{a})(\hat{b}^\dagger + \hat{b}), \quad (7)$$

where $\Delta = \omega_d - \omega_0$, $\hat{a}^\dagger(\hat{a})$ the creation (annihilation) operator for the cavity field variation and $\hat{b}^\dagger(\hat{b})$ the creation (annihilation) operator for the mechanical mode. The optomechanical coupling $g = g_0\sqrt{N}$ is enhanced by the number of photons N , g_0 being the single-photon coupling rate.

We obtain the Heisenberg-Langevin equations

$$\begin{aligned} \dot{\hat{a}}(t) &= \left(i\Delta - \frac{\kappa}{2}\right)\hat{a}(t) + ig(\hat{b}(t) + \hat{b}^\dagger(t)) + \sum_{j=e,0} \sqrt{\kappa_j}\hat{\xi}_j(t) \\ \dot{\hat{b}}(t) &= \left(-i\omega_m - \frac{\gamma_m}{2}\right)\hat{b}(t) + ig(\hat{a}(t) + \hat{a}^\dagger(t)) + \sqrt{\gamma_m}\hat{\xi}_m(t) \end{aligned}$$

and their Hermitian conjugates

$$\begin{aligned} \dot{\hat{a}}^\dagger(t) &= \left(-i\Delta - \frac{\kappa}{2}\right)\hat{a}^\dagger(t) - ig(\hat{b}(t) + \hat{b}^\dagger(t)) + \sum_{j=e,0} \sqrt{\kappa_j}\hat{\xi}_j^\dagger(t) \\ \dot{\hat{b}}^\dagger(t) &= \left(i\omega_m - \frac{\gamma_m}{2}\right)\hat{b}^\dagger(t) - ig(\hat{a}(t) + \hat{a}^\dagger(t)) + \sqrt{\gamma_m}\hat{\xi}_m^\dagger(t), \end{aligned}$$

where κ and γ_m are the decay rates of the cavity and the mechanical resonator respectively. The noise operators satisfy the following relationships: $\langle \hat{\xi}_m^\dagger(t)\hat{\xi}_m(0) \rangle = n_m^i\delta(t)$, $\langle \hat{\xi}_m(t)\hat{\xi}_m^\dagger(0) \rangle = (n_m^i + 1)\delta(t)$; $\langle \hat{\xi}_e^\dagger(t)\hat{\xi}_e(0) \rangle = n_e\delta(t)$, $\langle \hat{\xi}_e(t)\hat{\xi}_e^\dagger(0) \rangle = (n_e + 1)\delta(t)$; $\langle \hat{\xi}_0^\dagger(t)\hat{\xi}_0(0) \rangle = n_0\delta(t)$, $\langle \hat{\xi}_0(t)\hat{\xi}_0^\dagger(0) \rangle = (n_0 + 1)\delta(t)$; $n_e\kappa_e + n_0\kappa_0 = n_c\kappa$.

We will rewrite this in matrix form, setting

$$v(t) := \begin{pmatrix} \hat{a}(t) \\ \hat{a}^\dagger(t) \\ \hat{b}(t) \\ \hat{b}^\dagger(t) \end{pmatrix} \quad w(t) := \begin{pmatrix} \sum_{j=e,0} \sqrt{\kappa_j} \hat{\xi}_j(t) \\ \sum_{j=e,0} \sqrt{\kappa_j} \hat{\xi}_j(t) \\ \sqrt{\gamma_m} \hat{\xi}_m(t) \\ \sqrt{\gamma_m} \hat{\xi}_m(t) \end{pmatrix}$$

and

$$A := \begin{pmatrix} i\Delta - \frac{\kappa}{2} & 0 & ig & ig \\ 0 & -i\Delta - \frac{\kappa}{2} & -ig & -ig \\ ig & ig & -i\omega_m - \frac{\gamma_m}{2} & 0 \\ -ig & -ig & 0 & i\omega_m - \frac{\gamma_m}{2} \end{pmatrix}$$

thus we get

$$v'(t) = Av(t) + w(t).$$

Using Fourier transforms $\mathcal{F}(f(t)) = f(\omega) \equiv \int_{-\infty}^{\infty} f(t)e^{i\omega t} dt$ we have

$$-i\omega v(\omega) = Av(\omega) + w(\omega)$$

which has the solution

$$v(\omega) = (-i\omega I - A)^{-1} w(\omega) = B^{-1} w(\omega),$$

$$B = \begin{pmatrix} -i\omega - i\Delta + \frac{\kappa}{2} & 0 & -ig & -ig \\ 0 & -i\omega + i\Delta + \frac{\kappa}{2} & ig & ig \\ -ig & -ig & -i\omega + i\omega_m + \frac{\gamma_m}{2} & 0 \\ ig & ig & 0 & -i\omega - i\omega_m + \frac{\gamma_m}{2} \end{pmatrix} \\ \equiv \begin{pmatrix} 1/\chi_c & 0 & -ig & -ig \\ 0 & 1/\bar{\chi}_c & ig & ig \\ -ig & -ig & 1/\chi_m & 0 \\ ig & ig & 0 & 1/\bar{\chi}_m \end{pmatrix}.$$

For cooling we use $\Delta = -\Omega_m$ and let $\delta = \omega - \Omega_m$. Applying the rotating wave approximation, omitting contribution from $\bar{\chi}_c, \bar{\chi}_m$, we get

$$\hat{a}(\omega) = \frac{\chi_c \sum \sqrt{\kappa_i} \hat{\xi}_i + ig\chi_m\chi_c\sqrt{\gamma_m}\hat{\xi}_m}{1 + g^2\chi_c\chi_m} \quad (8)$$

$$\hat{b}(\omega) = \frac{\chi_m\sqrt{\gamma_m}\hat{\xi}_m + ig\chi_m\chi_c \sum \sqrt{\kappa_j} \hat{\xi}_j}{1 + g^2\chi_c\chi_m}. \quad (9)$$

From the input-output theory the output field can be expressed as

$$\begin{aligned} \hat{a}_{\text{out}} &= \hat{\xi}_e - \sqrt{\kappa_e}\hat{a} \\ &= \left(1 - \frac{\chi_c\kappa_e}{1 + g^2\chi_c\chi_m}\right) \hat{\xi}_e - \frac{\chi_c\sqrt{\kappa_e\kappa_0}}{1 + g^2\chi_c\chi_m} \hat{\xi}_0 - \frac{i\sqrt{\kappa_e\gamma_m}g\chi_c\chi_m}{1 + g^2\chi_c\chi_m} \hat{\xi}_m. \end{aligned} \quad (10)$$

Since a cancelling tone is added, the detected field is modified as

$$\begin{aligned} \hat{a}_{\text{out}} &= \hat{\xi}_e - \sqrt{\kappa_e}\hat{a} - \hat{\xi}_e \\ &= \frac{\chi_c\kappa_e}{1 + g^2\chi_c\chi_m} \hat{\xi}_e - \frac{\chi_c\sqrt{\kappa_e\kappa_0}}{1 + g^2\chi_c\chi_m} \hat{\xi}_0 - \frac{i\sqrt{\kappa_e\gamma_m}g\chi_c\chi_m}{1 + g^2\chi_c\chi_m} \hat{\xi}_m \\ &= \sum_{k=e,0,m} f_k(\omega) \hat{\xi}_k(\omega). \end{aligned} \quad (11)$$

The spectrum analyser detects the symmetric power spectral density (PSD) [7]

$$\begin{aligned} \frac{S(\omega)}{\hbar\omega} &= \frac{1}{2} \int_{-\infty}^{\infty} e^{i\omega t} \langle \hat{a}_{\text{out}}^\dagger(0) \hat{a}_{\text{out}}(t) + \hat{a}_{\text{out}}(t) \hat{a}_{\text{out}}^\dagger(0) \rangle dt \\ &= \frac{1}{2\pi} \frac{1}{2} \langle \hat{a}_{\text{out}}^\dagger(-\omega) \hat{a}_{\text{out}}(\omega) + \hat{a}_{\text{out}}(\omega) \hat{a}_{\text{out}}^\dagger(-\omega) \rangle. \end{aligned} \quad (12)$$

Strictly speaking this is for the lab frame, however in this case only the detunings enter the equations, therefore we could directly substitute in Supplementary Equation 8 and 11 and get

$$\frac{S(\omega)}{\hbar\omega} = \sum_{k=e,0,m} |f_k(\omega)|^2 \left(n_k^i + \frac{1}{2} \right), \quad (13)$$

$n_{e,0}^i$ being equivalent to $n_{e,0}$. Including the added noise from the amplification chain, we get

$$\frac{S(\omega)}{\hbar\omega} = \frac{g^2\kappa_e\gamma_m}{|g^2 + (\frac{\kappa}{2} - i\delta)(\frac{\gamma_m}{2} - i\delta)|^2} \left(n_m^i + \frac{1}{2} \right) + \frac{|\frac{\gamma_m}{2} - i\delta|^2\kappa_e\kappa}{|g^2 + (\frac{\kappa}{2} - i\delta)(\frac{\gamma_m}{2} - i\delta)|^2} \left(n_c + \frac{1}{2} \right) + n_{\text{add}}. \quad (14)$$

Note that the noise operators in the frequency domain satisfy the following relations:

$$\langle \hat{\xi}_k^\dagger(\omega) \hat{\xi}_k(\omega') \rangle = 2\pi n_k^i \delta(\omega + \omega'), \quad \langle \hat{\xi}_k(\omega) \hat{\xi}_k^\dagger(\omega') \rangle = 2\pi(n_k^i + 1) \delta(\omega + \omega').$$

The final occupation can be found via equipartition [4, 5]:

$$\begin{aligned}
1 + 2n_m &= \frac{\langle \hat{x}^2 \rangle}{x_{\text{zpf}}^2} = \int_{-\infty}^{\infty} \frac{d\omega}{2\pi} \frac{S_{xx}(\omega)}{x_{\text{zpf}}^2} \\
&= \frac{1}{x_{\text{zpf}}^2} \int_{-\infty}^{\infty} \frac{d\omega}{2\pi} \int_{-\infty}^{\infty} \frac{1}{2} \langle \hat{x}(t)\hat{x}(0) + \hat{x}(0)\hat{x}(t) \rangle e^{i\omega t} dt,
\end{aligned} \tag{15}$$

where $\hat{x}(t) = x_{\text{zpf}}(\hat{b}(t) + \hat{b}^\dagger(t))$, x_{zpf} being the zero-point fluctuation. Substituting in Supplementary Equation 9, using formulae of contour integrals and considering $\kappa^2 \gg 4g^2, \kappa\gamma_m, \gamma_m$, we find

$$n_m \approx \frac{\kappa\gamma_m}{4g^2 + \kappa\gamma_m} n_m^i + \frac{4g^2}{4g^2 + \kappa\gamma_m} n_c = \frac{1}{C+1} n_m^i + \frac{C}{C+1} n_c. \tag{16}$$

Supplementary Note 7: Noise from the signal generator

For the measurement shown in Fig. 4 of the main text, we use a Phase Matrix QuickSyn FSW-0020 microwave signal generator. We measure a sideband noise S_ϕ of -130 dBc/Hz at 120 kHz offset for a 5.1 GHz carrier signal. Cavity noise occupancy n_c contributed by the signal's own noise can be estimated by

$$n_c = \frac{P_{\text{in}} S_\phi \cdot \kappa_e}{\hbar\omega} \frac{\kappa_e}{(\kappa/2)^2}. \tag{17}$$

For a critically coupled cavity, we have

$$n_c = \frac{P_{\text{in}} \times 10^{-13}/\text{Hz}}{\hbar\omega}. \tag{18}$$

The green line in Fig. 4c in the main text is plotted with the above equation.

Measurements were also performed using an Agilent PSG-UNY low phase noise option microwave signal generator which was available to us for a short time. Although the phase noise of the PSG-UNY at an offset of 120 kHz is specified to be -137 dBc/Hz for 5 GHz carrier signals, the total sideband noise (amplitude and phase) was observed to be -132 dBc/Hz. Although we did not have time to perform a full thermal calibration of the setup with the PSG-UNY, we observed that the cavity noise n_c was about 2 dB lower with the PSG generator with no evidence of additional mode heating, implying that the final occupation with the PSG generator would be 4.3 phonons.

Supplementary References

- [1] Singh, V. *et al.* Optomechanical coupling between a multilayer graphene mechanical resonator and a superconducting microwave cavity. *Nat. Nanotechnol.* **9**, 820–824 (2014).
- [2] Aspelmeyer, M., Kippenberg, T. J. & Marquardt, F. Cavity optomechanics. *Rev. Mod. Phys.* **86**, 1391–1452 (2014).
- [3] Marquardt, F., Chen, J., Clerk, A. & Girvin, S. Quantum theory of cavity-assisted sideband cooling of mechanical motion. *Phys. Rev. Lett.* **99**, 093902 (2007).
- [4] Dobrindt, J. M., Wilson-Rae, I. & Kippenberg, T. J. Parametric normal-mode splitting in cavity optomechanics. *Phys. Rev. Lett.* **101**, 263602 (2008).
- [5] Rocheleau, T. *et al.* Preparation and detection of a mechanical resonator near the ground state of motion. *Nature* **463**, 72–75 (2010).
- [6] Teufel, J. D. *et al.* Sideband cooling of micromechanical motion to the quantum ground state. *Nature* **475**, 359–363 (2011).
- [7] Clerk, A. A., Devoret, M. H., Girvin, S. M., Marquardt, F. & Schoelkopf, R. J. Introduction to quantum noise, measurement, and amplification. *Rev. Mod. Phys.* **82**, 1155–1208 (2010).
- [8] Gorodetsky, M. L., Schliesser, A., Anetsberger, G., Deleglise, S. & Kippenberg, T. J. Determination of the vacuum optomechanical coupling rate using frequency noise calibration. *Opt. Express* **18**, 23236–23246 (2010).